To be published in Optics Letters:

Title:	Polarization fading mitigation in distributed acoustic sensors based on a high-speed polarization rotator
Authors:	Shahab Bakhtiari Gorajoobi,Ali Masoudi,Gilberto Brambilla
Accepted:	11 January 22
Posted	12 January 22
DOI:	https://doi.org/10.1364/OL.450388

Polarization fading mitigation in distributed acoustic sensors based on a high-speed polarization rotator

SHAHAB BAKHTIARI GORAJOOBI[*,1], ALI MASOUDI[1], AND GILBERTO BRAMBILLA[1]

[1] Optoelectronics Research Centre, University of Southampton, Southampton, SO17 1BJ, UK
[*] Corresponding author: sbg1v17@soton.ac.uk

Compiled January 11, 2022

A distributed optical fiber acoustic sensor based on interferometric demodulation technique with no polarization fading is demonstrated. A polarization diversity scheme based on high-speed polarization rotator is used to eliminate signal fading due to polarization mismatch in the Rayleigh backscattered signal between adjacent points on the sensing fiber. This technique yields a spatially uniform response to the applied strain. The sensor exhibited a spatial and strain resolutions of <4 m and $<$7 nε, respectively.

http://dx.doi.org/10.1364/ao.XX.XXXXXX

Phase-sensitive Optical Time-domain Reflectometry (ϕ-OTDR) enables quantification of dynamic strains along an optical fiber by analyzing the phase of the Rayleigh backscattered light from an optical pulse launched into the fiber [1]. Such technology forms the basis of Distributed Acoustic Sensors (DASs), which are employed to monitor pipelines, cables, infrastructures and seismic events [2–7]. Measurement fidelity of DASs has increased in importance as industries progressively demanded systems with improved range, resolution, and sensitivity. Signal fading, as one of the hallmarks of DAS systems, plays an adverse role in the measurement fidelity.

DASs suffer from three types of signal fading: intensity, phase, and polarization fading. Intensity fading occurs when the backscattered electromagnetic waves from inhomogeneities at a given section of the sensing fiber are destructively added to one another reducing the intensity of the backscattered light from that section to a level close to zero. Phase fading occurs when the phase-difference between the backscattered lights from two segments on the fiber, separated by the gauge length is $N\pi$ where N is an integer. In such scenario, where the superposition of the backscattered signals is at a maxima or minima of the interferometric pattern, a small strain variation over the said gauge length results in minute intensity changes at the output of the interferometer which, in turn, translates into signal fading. Finally, in direct detection DAS systems, polarization fading occurs when the polarization of backscattered lights from two ends of the said gauge length are orthogonal. Since lights with orthogonal polarizations do not mix, no interferometric pattern is formed at the output of the interferometer which, subsequently, results in signal fading. In coherent detection DAS systems, on the other hand, polarization fading occurs when the polarization state of the optical local oscillator signal is orthogonal to that of the backscattered light.

To eliminate intensity fading, Hartog et al. proposed a frequency diversity interrogation technique [8], in which the frequency of the seed laser is up-shifted in several steps to create several statistically independent Rayleigh backscattered traces with different coherent Rayleigh noise patterns. By combining the measurements from the Rayleigh backscattered traces acquired at different frequencies, it is possible to eliminate the intensity fading while increasing the sensing precision, albeit at the cost of reduced measurement bandwidth. All other coherent DAS systems that have been developed to eliminate intensity fading are based on the same concept, but with different implementations [9–12].

Techniques adopted for eliminating phase fading are tailored to the DAS sensing approach [2, 13]. Interferometric DAS systems, for instance, use two approaches: 1) a 3×3 coupler to create three signals $2\pi/3$ out of phase [14–16] and 2) phase generated carrier which relies on the modulation of the phase of light in one arm of the interferometer and its mixture with the light from the other arm to generate a beat signal [17, 18]. For dual-pulse DAS systems, the phase fading has been eliminated by shifting the phase difference between subsequent pulse-pairs by $2\pi/3$, but at the cost of reduced measurement bandwidth [19]. For coherent DAS systems, a commonly used technique is based on a 90° hybrid [20–22].

Polarization fading is less of an issue for direct detection DAS systems with a relatively short gauge lengths, especially those relying on a straight Single Mode Fibers (SMFs) with a relatively low birefringence over the gauge length of the DAS system [3, 23–25]. However, for applications that are based on wound fibers such as distributed optical fiber hydrophones [26] or helically-wound fiber optic cables used in vertical seismic profiling [27], polarization fading might result in a substantial signal fading. So far, only coherent DAS systems have addressed polarization fading through polarization diversity detection [21, 28]. In this technique, a polarization beam splitter is used to split the backscattered light into two orthogonal polarizations and the phase information at each State of Polarization (SoP) is obtained through coherent detection. Polarization diversity approach, however, requires twice as many balance detectors (the total of four balanced detectors in the case of dual polarization 90° hybrid) and may yield lower SNR due to the additional losses

from the addition of polarization beam splitter.

In this study, a new sensing arrangement based on a high-speed polarization rotator is proposed to mitigate polarization fading in an interferometric DAS system. The polarization rotator is added in one arm of an Imbalanced Mach-Zehnder Interferometer (IMZI) to rotate the polarization of the light between two orthogonal states before mixing it with the light in the other arm. The implementation of polarization diversity scheme has yielded a more uniform strain measurement with lower signal distortion and better strain accuracy.

The sensing principle of an interferometric DAS with polarization diversity provision is, for most part, similar to that of a conventional interferometric DAS. In conventional interferometric DAS, the dynamic strain at any given section of the sensing fiber is measured by mixing the backscattered light from the two ends of that section and evaluating the variation in the phase of the mixed light [14]. To mix the light from different points on the fiber that are separated by the gauge length, an IMZI with a path difference twice that of the gauge length is used. However, since the birefringence induced by fiber imperfections changes the polarization state of the light, there might be sections along the sensing fiber, separated by the gauge length, where the backscattered signals do not mix properly (Fig. 1(a)). To address this issue, a polarization rotator can be incorporated in the IMZI to sequentially rotate the polarization of the light in one arm of the interferometer between 0° and 180° on the Poincaré sphere before combining it with the light from the other arm (Fig. 1(b)). By adopting this sensing arrangement, it can be guaranteed that the light from any given points on the fiber that are separated by the gauge length will be mixed with one another. Hence, by combining the data from two SoPs through, for instance, calculating the weighted average of the data obtained from two SoPs, the polarization fading can be eliminated.

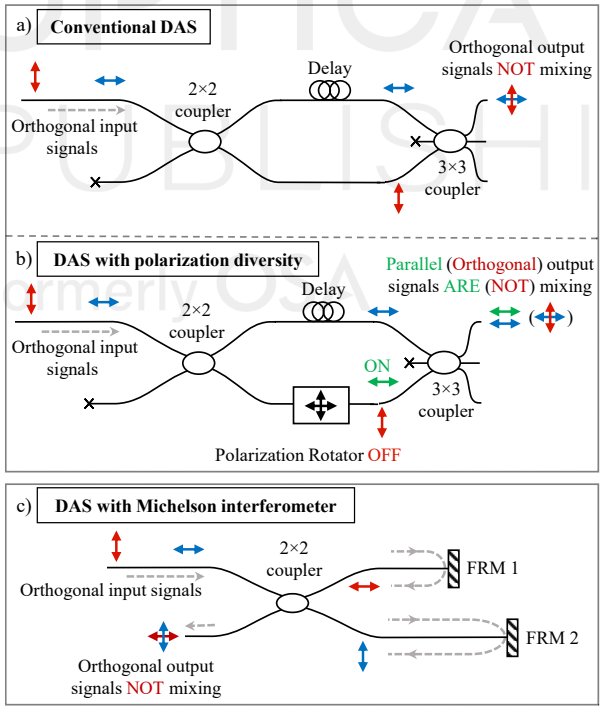

Fig. 1. a) Demonstration of a conventional MZI demodulation technique suffering from polarization fading when orthogonal signals from separated points on the fiber mix. b) MZI with integrated polarization rotator at off and on states eliminating polarization fading at the output of the 3×3 coupler, and c) schematic of a MI demodulation technique using Faraday Rotating Mirrors (FRMs) suffering from polarization fading when signals with orthogonal polarizations enter the two arms of the interferometer and mix with the same polarizations state at the output 2×2 coupler.

It should be noted that interferometric DAS systems that use Michelson Interferometer (MI) at their receiving arm are still susceptible to polarization fading [15, 17, 18]. As schematically shown in Fig. 1(c), MI does not address the polarization fading issue that may occur due to orthogonal SoP of the backscattered lights. A MI can only address polarization fading within the interferometer.

The experimental setup used in this study is shown in Fig. 2. A 1550 nm Continuous-wave (CW) laser diode with 10 mW mean power is intensity modulated by an Electro-optic Modulator (EOM) to generate 40 ns pulses at a repetition rate of 10 kHz. Each pulse passes through an optical isolator and then amplified using an Erbium-doped Fiber Amplifier (EDFA1). An Acousto-optic Modulator (AOM) with >50 dB extinction ratio is used as a pulse picker. A tap coupler is employed to monitor the pulse power and profile. The SoP of the pulse entering the test fiber is altered using a polarization controller to stimulate polarization states that induce signal fading. The probe pulse with 145 mW peak power is launched into the test fiber via circulator C1. The test fiber includes 8.5 km of SMF (Corning SMF-28) spliced to 1.7 m of fiber wound around a Piezoelectric Transducer (PZT). To induce high birefringence, a PZT with 38 mm outer diameter is used to impose strain on the fiber. An 80 m long SMF is added to the fiber on the PZT to separate the test region from the far-end of the sensing fiber. The optical circulator C1 directs the backscattered light into the receiving arm of the setup. At this stage, EDFA2 amplifies the signal which is then filtered using a Fiber Bragg Grating (FBG) filter with a

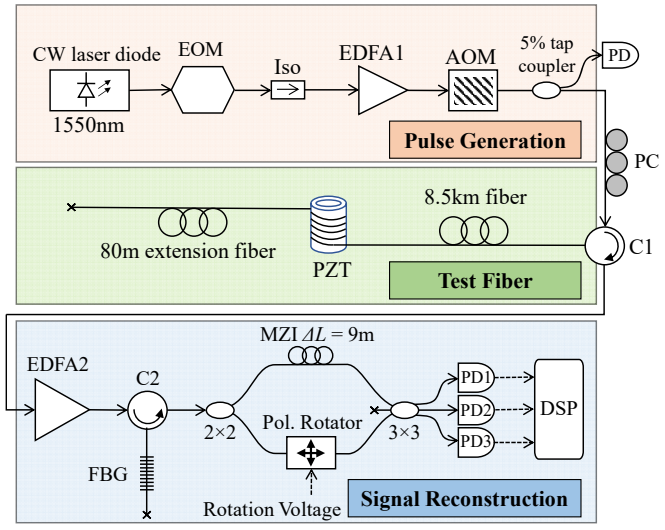

Fig. 2. Experimental setup. CW: Continuous-wave, EOM: Electro-optic Modulator, EDFA: Erbium-doped fiber amplifier, AOM: Acousto-optic Modulator, PC: Polarization Controller, C: Circulator, PZT: Piezoelectric Transducer, FBG: Fiber Bragg Grating, MZI: Mach Zehnder Interferometer, PD: Photodetector.

reflectivity and bandwidth of 59% and 0.03 nm, respectively. A MZI with a path imbalance of $\Delta L = 9$ m is adapted to accommodate a polarization rotator (Lightwaves2020: PR0-HSP0C) in one of its arms. A symmetric 3×3 coupler is spliced to the two arms of the MZI at one end and to three Photodetectors (PDs) with 125 MHz bandwidth at the other end [29]. A digitizer with 500 MHz bandwidth is used to acquire the output voltages of the PDs.

The polarization rotator is programmed to shift the SoP of the light in one arm of the interferometer by 180° on the Poincaré Sphere for every other backscattered traces. Figures 3(a) and 3(b) show a schematic plot of the OTDR traces and the switching sequence of the polarization rotator. A demodulation scheme based on arctangent function is used to extract the phase information from the Rayleigh backscattered traces [14].

The polarization rotator performs as a variable quarter-wave plate retarder. Figure 4(a) plots the response of the polarization rotator to a light wave with an arbitrary initial SoP of s on the Poincaré sphere, where S1-S3 denote the Stokes parameters in Cartesian coordinates. For any point on the Poincaré sphere, the polarization rotator transforms the SoP to its corresponding diametrical point on the circle of rotation. Figure 4(b) shows the backscattered traces at the output of the MZI obtained at OFF (blue trace) and ON (orange trace) state of the polarization rotator along a 110 m-section of the test fiber. The two traces show that the polarization of the backscattered Rayleigh light at the output of the MZI can have near orthogonal polarizations which can cause polarization fading since orthogonal signals do not interfere. At other positions, no significant fading can be observed due to presence of non-orthogonal polarization components in the combined waves. It should be noted that the polarization rotator applies a fixed phase-shift on the signal. However, since such phase-shift has a constant value, it has no effect on the analysis of the dynamic phase.

To implement the polarization diversity scheme shown in Fig. 3, the OTDR traces with the same SoP are analyzed together. This reduces the effective sampling rate of the sensor by a factor of two down to 5 kHz. Figure 5 plots the response of the DAS system to a sinusoidal strain wave imposed on a sensing fiber interrogated by probe pulses with three different SoPs. The amplitude and frequency of the strain wave was set to 1 $\mu\varepsilon$ and 10 Hz, respectively. Figures 5(a) and 5(b) show the output of the DAS at two states of the polarization rotator. The amplitude of Fast Fourier Transforms (FFTs) of both waterfall plots are shown in Fig. 5(c). Results show that the visibility of the signal is de-

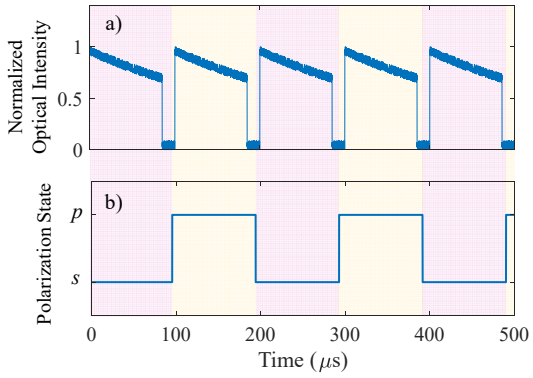

Fig. 3. Schematic of (a) OTDR traces, and (b) corresponding polarization state of the polarization rotator.

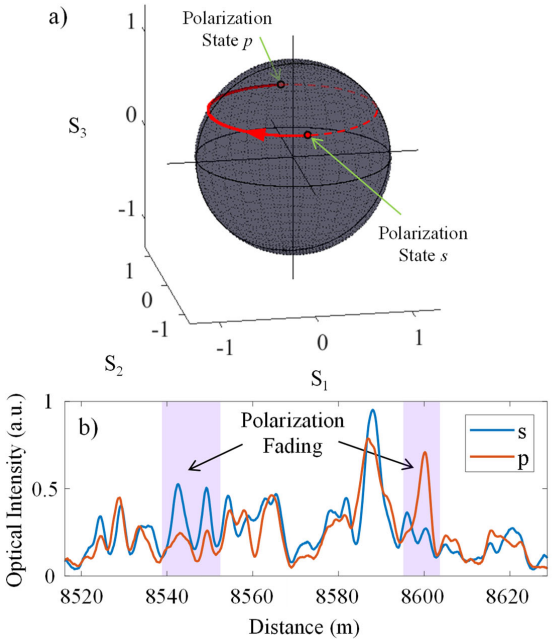

Fig. 4. (a) Example of the performance of the polarization rotator form the polarimetry experiment when an arbitrary SoP of s on the Poincaré sphere is rotated to its corresponding diametrical point resulted in SoP of p (solid red line), and (b) The OTDR traces at the end of the test fiber corresponding to the two SoPs of s and p showing the polarization fading effect can occur at certain positions along the fiber.

teriorated at few points along the sensing fiber for both s and p SoPs due to polarization fading (noticeably at 8622m in Fig. 5(a) and 8620 m in Fig. 5(b)). Using the FFT amplitudes, a weighted average of both results was used to calculate the strain. The reconstructed phase, $\Delta\phi\,(s,p)$, can be obtained from the individual phases, $\Delta\phi\,(s)$ and $\Delta\phi\,(p)$ for s and p SoPs, respectively, such that

$$\Delta\phi(s,p) = \frac{|FFT(s)| \times \Delta\phi(s) + |FFT(p)| \times \Delta\phi(p)}{|FFT(s)| + |FFT(p)|} \quad \textbf{(1)}$$

where $|FFT(s)|$ and $|FFT(p)|$ denote the amplitude of FFTs at s and p SoPs, respectively. Note that there are other signal aggregation techniques that do not rely on the FFT of the signal. Figure 5(d) shows the reconstructed data using Eq. (1). The reconstructed signal shows a uniform response along the sensing fiber where the strain is applied with no significant signal distortion. Changes in the polarization of the probe pulse can alter the level of the polarization fading along the fiber. Data set 2 plotted in Figs. 5(e-h) shows that polarization fading only occurs for the p SoP (see Figs. 5(e) and 5(f) at 8620 m). Similarly, the obtained reconstructed signal shows an improved performance. The third data set plotted in Figs. 5(i-l) demonstrates that polarization fading may not occur. Combining the data from two states of polarization (Figs. 5(i) and 5(j)) can lower the noise floor in the region where there is no vibration for the reconstructed signal (Fig. 5(l)), hence, improving the resultant SNR.

Figure 6 plots the FFT of the reconstructed signal for data set 2. It shows that the spatial resolution of the sensor is less than 4 m and the measured sensing precision is <7 $n\varepsilon$.

In summary, a DAS system based on a polarization diversity scheme was developed. Polarization diversity was achieved by

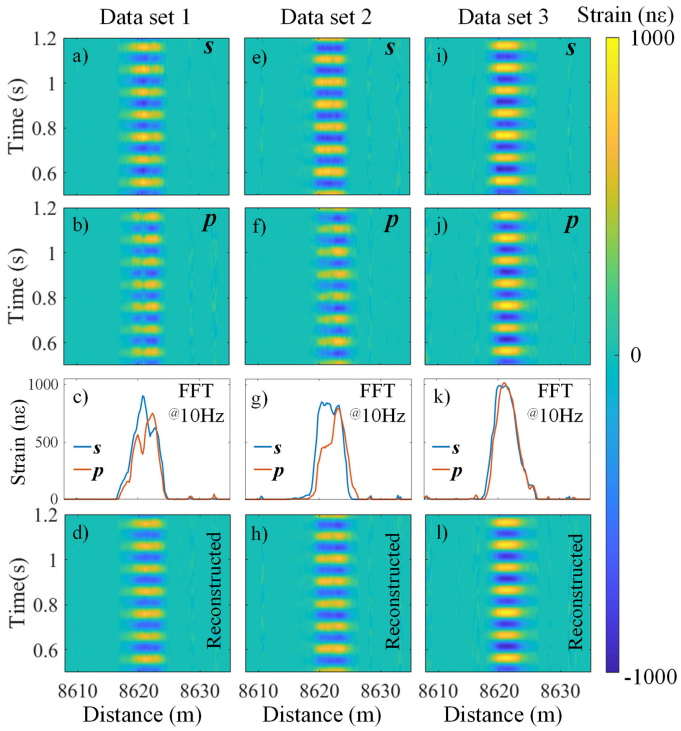

Fig. 5. Characterization of the DAS sensor using a sinusoidal strain wave with frequency and amplitude of 10 Hz and 1 $\mu\varepsilon$ for three cases: 1) data set 1: polarization fading at both (a) s, and (b) p states, (c) corresponding FFTs, and (d) reconstructed signal; 2) data set 2: no polarization fading at (e) s state, but polarization fading at (f) p state, (g) corresponding FFTs, and (h) reconstructed signal; and 3) data set 3: no polarization fading at both (i) s, and (j) p polarization switching states, (k) corresponding FFTs, and (l) reconstructed signal using a weighted average.

embedding a high-speed polarization rotator in one arm of the MZI, which rotated the SoP of the light by 180° on the Poincaré sphere. Experimental results showed that when polarization fading occurs for either rotated or unrotated SoPs, a weighted average of the data obtained at both SoPs can be used to improve the measurement precision of the sensor. The sensor had <4 m spatial resolution and 8.5 km sensing range. Strain variations at the frequency of 10 Hz were measured with a precision of <7 nε. This method can be used in conjunction with frequency diversity scheme to eliminate all signal fadings in a DAS system. Additionally, further improvements can be achieved by incorporating multiple SoPs at the cost of a decreased bandwidth.

Funding. Royal Society (CHL/R1/180350); Natural Environment Research Council (NE/S012877/1, NE/T005890/1).

Disclosures. The authors declare no conflicts of interest.

Data availability. Openly available at 10.5258/SOTON/D2078.

REFERENCES

1. A. Masoudi, M. Belal, and T. P. Newson, Meas. Sci. Technol. **24**, 085204 (2013).
2. A. Masoudi and T. P. Newson, Rev Sci Instrum **87**, 011501 (2016).
3. A. Masoudi, J. A. Pilgrim, T. P. Newson, and G. Brambilla, J. Light. Technol. **37**, 1352 (2019).

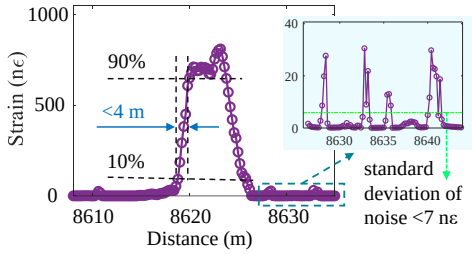

Fig. 6. FFT of the reconstructed signal for data set 2 at 10 Hz showing the spatial distribution of the applied strain along the fiber. The spatial resolution and measurement precision are <4 m and <7 nε, respectively. Inset shows the noise variations along the fiber where there is no vibration.

4. Z. W. Ding, X. P. Zhang, N. M. Zou, F. Xiong, J. Y. Song, X. Fang, F. Wang, and Y. X. Zhang, J. Light. Technol. **39**, 5163 (2021).
5. A. Lellouch and B. L. Biondi, Sensors (Basel) **21**, 2897 (2021).
6. R. Law, P. Christoffersen, B. Hubbard, S. H. Doyle, T. R. Chudley, C. M. Schoonman, M. Bougamont, B. d. Tombe, B. Schilperoort, C. Kechavarzi, A. Booth, and T. J. Young, Sci. Adv. **7**, eabe7136 (2021).
7. T. S. Hudson, A. F. Baird, J. M. Kendall, S. K. Kufner, A. M. Brisbourne, A. M. Smith, A. Butcher, A. Chalari, and A. Clarke, J. Geophys. Res. Solid Earth **126** (2021).
8. A. H. Hartog, L. B. Liokumovich, N. A. Ushakov, O. I. Kotov, T. Dean, T. Cuny, A. Constantinou, and F. V. Englich, Geophys. Prospect. **66**, 192 (2018).
9. J. Gu, B. Lu, J. Yang, Z. Wang, L. Ye, Q. Ye, R. Qu, and H. Cai, IEEE Photonics J. **12**, 1 (2020).
10. M. Zabihi, Y. Chen, T. Zhou, J. Liu, Y. Shan, Z. Meng, F. Wang, Y. Zhang, X. Zhang, and M. Chen, J. Light. Technol. **37**, 3602 (2019).
11. H. M. Ogden, M. J. Murray, J. B. Murray, C. Kirkendall, and B. Redding, Sci Rep **11**, 17921 (2021).
12. S. Guerrier, C. Dorize, E. Awwad, and J. Renaudier, Opt Express **29**, 35149 (2021).
13. Y. Rao, Z. Wang, H. Wu, Z. Ran, and B. Han, Photonic Sensors **11**, 1 (2021).
14. A. Masoudi and T. P. Newson, Opt Lett **42**, 290 (2017).
15. C. Wang, C. Wang, Y. Shang, X. Liu, and G. Peng, Opt. Commun. **346**, 172 (2015).
16. S. K. Sheem, T. G. Giallorenzi, and K. Koo, Appl. Opt. **21**, 689 (1982).
17. G. Fang, T. Xu, S. Feng, and F. Li, J. Light. Technol. **33**, 2811 (2015).
18. Z. Yu, Q. Zhang, M. Zhang, H. Dai, J. Zhang, L. Liu, L. Zhang, X. Jin, G. Wang, and G. Qi, Appl. Phys. B **124** (2018).
19. A. E. Alekseev, V. S. Vdovenko, B. G. Gorshkov, V. T. Potapov, and D. E. Simikin, Laser Phys. **24** (2014).
20. Z. Wang, L. Zhang, S. Wang, N. Xue, F. Peng, M. Fan, W. Sun, X. Qian, J. Rao, and Y. Rao, Opt Express **24**, 853 (2016).
21. J. J. Mompo, L. Shiloh, N. Arbel, N. Levanon, A. Loayssa, and A. Eyal, J. Light. Technol. **37**, 4597 (2019).
22. Y. Wakisaka, D. Iida, H. Oshida, and N. Honda, J. Light. Technol. **39**, 4279 (2021).
23. D. Milne, A. Masoudi, E. Ferro, G. Watson, and L. Le Pen, Mech. Syst. Signal Process. **142**, 106769 (2020).
24. N. J. Lindsey and E. R. Martin, Annu. Rev. Earth Planet. Sci. **49**, 309 (2021).
25. D. Rivet, B. de Cacqueray, A. Sladen, A. Roques, and G. Calbris, J Acoust Soc Am **149**, 2615 (2021).
26. B. Lu, B. Wu, J. Gu, J. Yang, K. Gao, Z. Wang, L. Ye, Q. Ye, R. Qu, X. Chen, and H. Cai, Opt Express **29**, 3147 (2021).
27. B. N. Kuvshinov, Geophys. Prospect. **64**, 671 (2016).
28. C. Dorize, S. Guerrier, E. Awwad, and J. Renaudier, Opt Lett **46**, 2754 (2021).
29. M. Chen, A. Masoudi, and G. Brambilla, Opt Express **27**, 9684 (2019).